Particle-Stabilized Defect Gel in Cholesteric Liquid Crystals

Martin Zapotocky, Laurence Ramos, Philippe Poulin,*
T. C. Lubensky,† D. A. Weitz

Dispersions of colloidal particles in cholesteric liquid crystals form an unusual solid by stabilizing a network of linear defects under tension in the ideal layered structure of the cholesteric. The large length scales of the cholesteric liquid crystals allowed direct observation of the network structure, and its properties were correlated with rheological measurements of elasticity. This system serves as a model for a class of solids formed when particles are mixed with layered materials such as thermotropic and lyotropic smectic liquid crystals and block copolymers.

Lamellar phases (*1*), whose equilibrium state consists of a periodic stack of two-dimensional planes, occur in many materials, including thermotropic liquid crystals (LCs), surfactant-water and lipid-water mixtures, surfactant-water-oil mixtures, and block copolymers. In many cases, control of their rheology—their distortion, flow, and sedimentation under stress—is crucial to product performance in industries such as food, cosmetics, and coatings (*2*). The addition of colloidal particles can modify the rheological properties of a variety of complex fluids (*3*). Often, however, an incomplete understanding of structural modifications induced by inclusions has limited our ability to control and tune these properties. We show that the addition of a small volume fraction of colloidal particles to lamellar systems can efficiently control their rheology, and we present a detailed analysis of the relation between inclusion-induced microstructural changes and rheology modification.

We used a nearly ideal model lamellar system whose layer spacing can be varied and made sufficiently large to allow easy real-time optical visualization of both the lamellae orientation and the structure of any defects induced by the addition of colloidal particles. We studied cholesteric LCs (*1*), which have a twisted nematic structure in which anisotropic molecules rotate in a helical manner to form lamellae of equally spaced planes with a common molecular orientation (Fig. 1A) (*4*). The pure cholesteric structure behaves as a fluid when sheared along the lamellae. The addition of colloidal particles to a cholesteric LC, however, stabilized a network of linear defects under tension that is responsible for a solidlike response to shear stress. Because we can correlate direct visualization of the defect network with rheological measurements, we can probe quantitatively the mechanisms of elastic response. The resultant defect-mediated gel provides a model for predicting the consequences of the addition of colloidal particles to other lamellar phases. Indeed, the stabilization of a network of defects similar to that we describe here has been observed (*5*) in a lyotropic smectic system. In mesophases such as Sm*A* liquid crystals, block co-polymers, and lyotropic L_α phases, the formation of the defect network is expected to result in higher shear moduli than that in cholesteric LCs because of the smaller spacing between lamellae of these mesophases.

The defect-driven enhancement of the elastic modulus of lamellar systems, such as the one studied here, is intrinsically different from that obtained when colloidal particles are dispersed in systems, such as polymer solutions and melts (*3*, *6*), which have no long-range order and do not support defect structures. It is also different from the solid-like rigidity observed in macroscopically disordered samples of layered phases (*7*, *8*), whose origin is bulk regions with layers unfavorably aligned relative to the shear direction (*1*, *9*). This rigidity cannot survive shear-induced alignment of these randomly oriented regions; in contrast, colloidally stabilized defect networks and their solid-like elasticity are not destroyed by such shear alignment. Lamellar hydrogels (*10*) produced by the addition of a polymer surfactant to the lamellar phase of a phospholipid in water have a defect structure, which was imaged by freeze-fracture electron microscopy, similar to that reported here for colloidal particle in cholesterics. The mechanism for stabilization of their defect networks, however, relies on specific interactions between polymer and phospholipid, unlike the more general, purely physical mechanism reported here. Colloidal particles dispersed in a nematic LC gives rise to defects (*11*), but they have no effect on the bulk rheological properties, at least at small volume fractions.

To determine the effects of defects in the ideal cholesteric structure shown in Fig. 1A, we quenched from the isotropic (66°C) to the cholesteric (55°C) phase over several seconds. A large concentration of "oily streak" defects (Fig. 1, B and C) emerged at the phase transition temperature (63°C) and formed a dense network (Fig. 2, A to C). This network coarsened quickly; after 2 min, almost no defects were left in the sample with thickness $D_{film} = 40$ μm. The dominant coarsening mechanism is the disconnection of defect lines from the nodes of the network and their subsequent shrinking with a constant velocity (a retracting oily streak is visible in the upper left corner of Fig. 2C).

Dramatically different behavior was observed when the system was first doped with colloidal particles. We used silica particles with a diameter of ~1 μm. The particles formed clusters of typical diameter $R_{inc} \simeq 5$ to 20 μm, which then dispersed randomly. In the regime $p < R_{inc} < D_{film}$ (where p is the pitch length), cholesteric order (and consequently the organization of the layers) was strongly perturbed by the presence of the inclusions, but the boundary condition at the sample surface was not affected. The initial state, right after the quench, was indistinguishable from that of a pure cholesteric—a dense network of defects formed in both cases. Initially, the defects coarsened at the same rate as in the pure cholesteric. However, after about 1 min, the rate of coarsening dramatically decreased; subsequently, the characteristic mesh size d_{net} remained ≤200 μm for several hours. The colloidal inclusions were located preferentially at the nodes of the defect network (Fig. 2, D to F) and stabilized it.

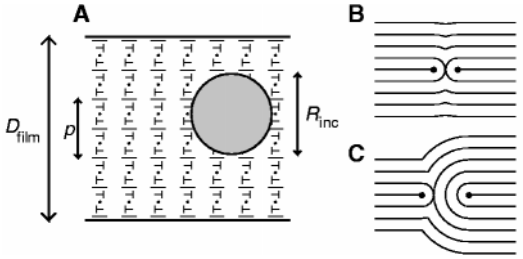

Fig. 1. (**A**) The planar texture configuration of a cholesteric liquid crystal. Structural modifications occur when colloidal inclusions of size R_{inc} exceeding the pitch length p are added into the system. (**B**) Arrangement of cholesteric layers in the cross section of a symmetric "oily streak" defect. The layers undergo a 180° rotation around each of the two constituent disclinations (shown as full circles) in the center of the streak. (**C**) An asymmetric oily streak, equivalent (at large distances from the center of the streak) to a dislocation with Burgers vector magnitude $b = 4$.

Department of Physics and Astronomy, University of Pennsylvania, Philadelphia, PA 19104, USA.

*Present address: Centre de Recherche Paul Pascal, Avenue A. Schweitzer, F-33600, Pessac, France.
†To whom correspondence should be addressed.

This stabilization appears to be quite general: It was unaffected by the replacement of silica particles with water droplets or by the modification of boundary conditions on the director at inclusion surfaces from parallel to perpendicular alignment. It is this stabilized network of oily streaks that provides the solidlike elasticity in our samples.

The simplest, symmetric oily streak (Fig. 1B) (*12*) is composed of two disclinations of equal sign, separated by two-layer spacings. This structure does not introduce a change in the number of layers—it is not a dislocation, and it is not topologically stable. It can terminate in the bulk and retract at one end, as is indeed seen during the process of coarsening (Fig. 2, C and E). In contrast, an asymmetric oily streak (Fig. 1C) is topologically equivalent to a dislocation with nonzero Burgers vector when viewed on scales larger than the thickness of the streak, s, defined as the distance between the two constituent disclinations. Asymmetric streaks are topologically stable and cannot terminate in the bulk.

To explain the dynamics of the defect structures, we treat the cholesteric as an incompressible layered mesophase, with a free-energy density given by

$$f_{\mathrm{lam}} = \tfrac{1}{2}K\left(\frac{1}{R_1}+\frac{1}{R_2}\right)^2 + \overline{K}\left(\frac{1}{R_1R_2}\right) \quad (1)$$

where R_1 and R_2 are the local values of the principal radii of curvature of the layers and K and $\overline{K}$ are, respectively, the mean and Gaussian bending rigidities of the layers. Here $K = (3/16)K_{33}$, where K_{33} is the standard elastic constant for bend deformations of the director (*13*). The Gaussian bending energy term, which integrates to boundaries, must be taken into account because our system contains internal surfaces and focal-conic type structures. The value of $\overline{K}$ can be estimated (*14*, *15*) from optical observations of focal conic structures in our samples as $\overline{K} = (1.5 \pm 0.3)K$. In the following, we take $\overline{K} = K \simeq 10^{-6}$ dyne.

In pure cholesterics and in cholesterics with inclusions at early times in the coarsening process, most of the defects are not stabilized by being connected to the nodes. The rate of coarsening is limited by the velocity of shrinking v of a typical disconnected streak, which was always observed to be constant in time. The value of v can be estimated theoretically as $4K/(\gamma_1 s)$, where γ_1 is the twist viscosity of the LC (*16*). Consistent with these properties of individual oily streaks, the total normalized optical density $A(t)$ of defects (defined as the ratio of dark to total area in digitized photographs such as Fig. 2) in pure cholesteric films decayed linearly with time (Fig. 3). As shown in the inset of Fig. 3, the time constant t_{dec} in $A(t) = 1 - t/t_{\mathrm{dec}}$ grew approximately exponentially with the film thickness, suggesting that the rate of coarsening becomes unobservably slow in bulk samples ($D_{\mathrm{film}} \geq 1$ mm).

The behavior in thin samples with colloidal inclusions was dramatically different; a sharp crossover (Fig. 3) between the linear decay of $A(t)$ and a nearly time-independent regime occurred at the time t_c when the typical spacing between the oily streaks became comparable to the average separation of inclusions. After this crossover time ($t_c \simeq 50$ to 100 s in our samples), most nodes of the oily streak network contained colloidal inclusions. The rate of coarsening was then limited by the rate at which the oily streaks disconnect from the nodes of the network, controlled in turn by the energy barrier for disconnection E_{disc} that reflects the presence of the inclusions at the nodes. As a result, the defect network was stabilized by the inclusions.

The following simplified picture may be used to provide a qualitative understanding of the nature of the interaction of colloidal inclusions with the oily streaks. An isolated inclusion is expected to be surrounded by a focal conic domain (*17*) that can be viewed as arising from a disclination ring lying on the surface of the inclusion. When the inclusion is located at the intersection of several symmetric oily streaks, parts of the disclination ring are eliminated. It is thus energetically favorable for the colloidal inclusions to be located at the nodes of the oily streak network. Disconnection of an oily streak from the inclusion must overcome an energy barrier with magnitude on the order of $(\pi/4)Ks$, where s is the thickness of the disconnecting streak. We consequently obtain the estimate $E_{\mathrm{disc}} \simeq Kp \simeq 10^{-9}$ erg for $p \simeq 10$ μm, and dimensional analysis leads us to expect the estimate $E_{\mathrm{disc}} \geq Kp \simeq \overline{K}p$ to be generally valid. E_{disc} exceeds the thermal energy k_BT by at least four orders of magnitude, so no thermally induced disconnections are expected to occur. Rather, it is the distribution of deformation stresses in the surrounding region of the network that will act as the driving force for overcoming E_{disc}. The structure of the network is, therefore, strongly history-dependent.

The particle-stabilized defect network should substantially modify the rheological

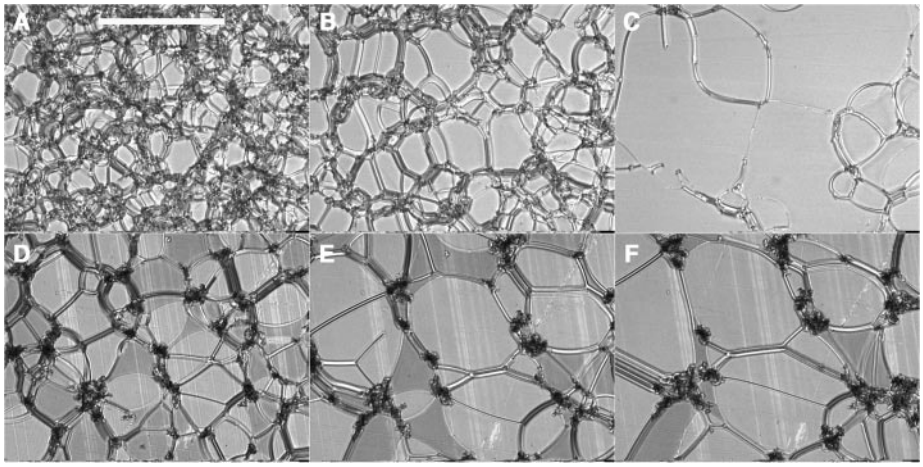

Fig. 2. (Upper row) Coarsening of the oily streak network in a pure cholesteric film with $p = 7$ μm and $D_{\mathrm{film}} = 40$ μm [at times (**A**) $t = 15$, (**B**) $t = 30$ s, and (**C**) $t = 75$ s after the quench] and in the same film with added colloidal inclusions [(**D**) $t = 1$ min, (**E**) $t = 4$ min, and (**F**) $t = 7$ min after the quench]. Imaging was performed with crossed polarizers; bar, 250 μm.

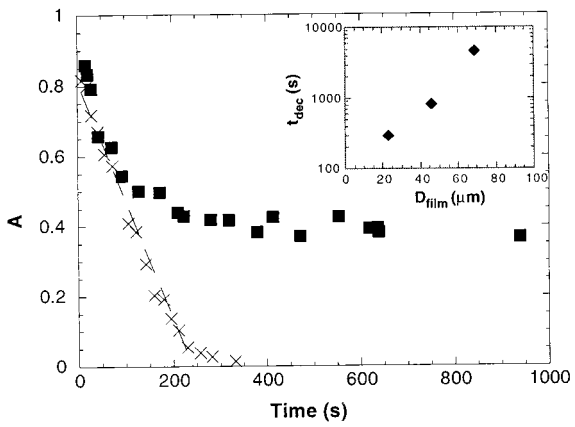

Fig. 3. The optical density $A(t)$ of defects at time t after the quench from isotropic to cholesteric phase in a sample of thickness $D_{\mathrm{film}} = 23$ μm (crosses: pure cholesteric; squares: cholesteric with inclusions). (**Inset**) The time constant t_{dec} in the linear regime $A(t) = 1 - t/t_{\mathrm{dec}}$, plotted as a function of D_{film}.

properties of the cholesteric fluid. On appropriate time scales (longer than the characteristic director relaxation time $\tau_{dir} \simeq (\gamma_1/K)(p/4\pi)^2$ at the cholesteric Brillouin zone edge and shorter than the typical lifetime of the network nodes), the defect structure can be viewed as a cross-linked network of elastic bonds that exert forces determined by the line tension $\mathcal{T}$ (the free energy per unit length) of the defects. Consequently, we expect the material to exhibit gel-like rheological behavior. This material exists solely because of the defect network; thus, it is a defect-mediated solid (*18*). The solid-like elasticity was evidenced in optical observations of a large air bubble moving through a thin sample: The defect network underwent strong transverse compression in the vicinity of the moving bubble; once the bubble moved away, however, the network rebounded to its original configuration (*19*).

The elastic shear modulus at low frequencies, G_0', of this network can be estimated theoretically with arguments analogous to those used in the theory of rubber elasticity (*20*). These suggest that $G_0' \simeq \mathcal{T}/d_{net}^2$, where d_{net} is the average mesh size of the defect network. Taking $\mathcal{T} \simeq 10K \simeq 10^{-5}$ dyne (*14*, *16*) and $d_{net} = 100$ μm, we obtain $G_0' \simeq 0.1$ dyne/cm^2, which corresponds to an extremely weak gel.

We compared the experimentally measured rheological properties of a pure cholesteric material with those of a cholesteric containing a 0.3% volume fraction of silica particles (*21*). Through strong preshearing (applying a constant shear of rate 10 s^{-1} for 500 s), we created well-aligned bulk samples whose morphology is similar to that of samples studied in optical observations discussed above and whose elasticity is dominated by the linear defect network (*22*).

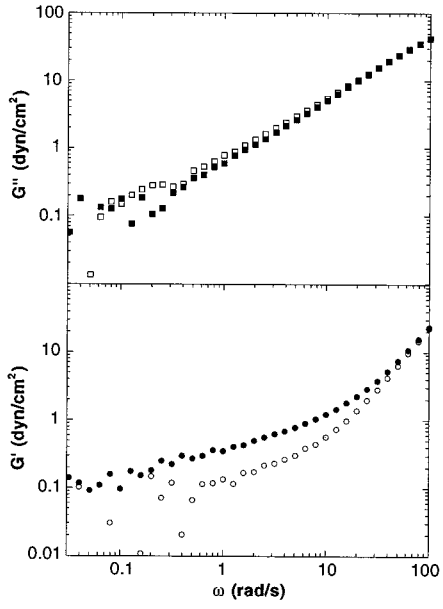

Fig. 4. Loss modulus (G'', squares) and storage modulus (G', circles) in the presheared cholesteric samples. The empty and filled symbols correspond to a sample without and with inclusions, respectively.

The pure cholesteric exhibited a liquid-like response in a wide range of frequencies, as shown in Fig. 4. For $\omega \geq 10$ rad/s, we observed typical Maxwell-fluid behavior: $G''(\omega) = \omega\eta$ with effective viscosity $\eta = 43$ *cp* and $G'(\omega) = \omega^2\eta\tau$ with relaxation time $\tau = 5.6$ ms. The value of τ agrees well with the characteristic director relaxation time $\tau_{dir} = (\gamma_1/K)(p/4\pi)^2 \simeq 6.1$ ms.

In a cholesteric with added colloidal particles, the Maxwell-fluid behavior persisted for $\omega \geq 50$ rad/s. At lower frequencies, however, the storage modulus $G'(\omega)$ exhibited a pronounced increase (by a factor of 3 to 4) compared with the pure cholesteric case (Fig. 4). This reflects the elasticity of the oily streak defects present in the sample with colloidal particles. Below $\omega = 1$ rad/s, we observed a plateau in the storage modulus $G'(\omega)$ of magnitude $G_0' = 0.2$ dyne/cm^2. Furthermore, the curves for $G'(\omega)$ and $G''(\omega)$ cross at $\omega \simeq \omega_g = 0.5$ rad/s, and to within experimental precision, $G'(\omega) > G''(\omega)$ for $\omega < \omega_g$. This provides a clear signature (*23*) of gel-like behavior and is consistent with our model of a particle-stabilized defect network. The value of G_0' is consistent with the prediction given above. In addition, ω_g agrees reasonably well with the estimated frequency $\mathcal{T}/(ud_{net}3\pi\gamma_1 R_{inc}) \simeq 2$ rad/s above which the maximum velocity $\omega u d_{net}$ of inclusions under oscillatory shear of amplitude $u = 0.05$ exceeds the velocity $\mathcal{T}/(3\pi\gamma_1 R_{inc})$ with which an oily streak can pull the inclusion (*24*).

For clarity, we contrast again the origins of solid-like elasticity in fully or partially disordered homogeneous lamellar systems with that in prealigned lamellar systems containing colloidal inclusions. In the latter system, regions where the layers are oriented at a nonzero angle with respect to shear are restricted to the vicinity of the colloidal inclusions and the centers of the oily streak defects. Such misaligned regions are widely separated by the well-aligned regions between the streaks; these well-aligned regions do not transmit elastic stress. This results in a highly inhomogeneous medium whose macroscopic solid-like elasticity arises from a connected network of oily streak defects that transmits elastic stresses only along the defect lines.

References and Notes

1. P.-G. de Gennes and J. Prost, *The Physics of Liquid Crystals* (Clarendon, Oxford, 1993).
2. R. Jowitt *et al*., Eds., *Physical Chemistry of Foods* (Applied Science, New York, 1983).
3. L. E. Nielsen and R. F. Landel, *Mechanical Properties of Polymers and Composites* (Dekker, New York, ed. 2, 1994), chap. 7.
4. We investigated cholesteric LCs with pitch p ranging from 0.5 to 15 μm, produced by doping a nematic consisting of a mixture of cyanobiphenyls with a small concentration of chiral molecules. Optical observations were carried out in thin films of width D_{film} ranging from 20 to 100 μm between microscope slides; thicker films lead to excessive light scattering and preclude the direct observation of their defect structure. The glass slides were coated with rubbed polyimide to enforce a parallel boundary condition at the surface for the nematic director, **n**, which specifies the average local orientation of the molecules. In this case, the lowest free-energy state of the pure cholesteric is the planar texture (*1*), characterized by horizontal layers connecting points of equal orientation of **n** (Fig. 1A). The cholesteric twist axis **t** in this configuration is oriented perpendicular to the film, and layers of equivalent orientation of **n** are spaced by the distance $h = p/2$.
5. P. Poulin and O. Mondain-Monval, unpublished data.
6. M. R. Kamal and A. Mutel, *J. Polym. Eng.* **5**, 293 (1985).
7. R. G. Larson *et al*., *Rheol. Acta* **32**, 245 (1993); S. Paasch, F. Schambil, M. J. Scwuger, *Langmuir* **5**, 1344 (1989).
8. R. H. Colby *et al*., *Rheol. Acta* **36**, 498 (1997).
9. K. Kawasaki and A. Onuki, *Phys. Rev. A* **42**, 3664 (1990).
10. H. E. Warriner *et al*., *Science* **271**, 969 (1996); *J. Chem. Phys.* **107**, 3707 (1997); S. L. Keller *et al*., *Phys. Rev. Lett.* **70**, 4781 (1997).
11. P. Poulin, H. Stark, T. C. Lubensky, D. A. Weitz, *Science* **275**, 1770 (1997).
12. See, for example, M. Kléman, *Points*, *Lines*, *and Walls* (Wiley, Chichester, UK, 1983).
13. T. C. Lubensky, *Phys. Rev. A* **6**, 452 (1972).
14. _____, P. Poulin, L. Ramos, D. A. Weitz, M. Zapotocky, in preparation.
15. P. Boltenhagen, O. Lavrentovich, M. Kléman, *J. Phys. II (Paris)* **1**, 1233 (1991).
16. The value of v is obtained from the balance of the line tension $\mathcal{T}$ (that is, the elastic energy per unit length) of the oily streak and of the viscous drag F acting at the end of the streak. We estimate $\mathcal{T}$ using a formalism similar to that of (*15*), and obtain (*14*) $\mathcal{T} \simeq \pi K \ln(s/p)$, with additional weak corrections due to the finite thickness of the film. Thus $\mathcal{T}$ depends only weakly on s; in the following, we omit the logarithmic factor in $\mathcal{T}$. The drag force acting on the disclination segment of length s terminating the oily streak is (up to logarithmic factors) $(\pi/4)s\gamma_1 v$. The condition $\mathcal{T} = F$ then gives $v = cs^{-1}$ with $c \simeq 4K/\gamma_1$. Taking the typical values $K = 10^{-6}$ dyne and $\gamma_1 = 100$ *cp*, we predict c to be of the order of 400 μm^2/s. Indeed, in a sample with cholesteric pitch $p = 7$ μm (and $D_{film} = 40$ μm), measurements of v for isolated oily streaks of thicknesses $s = p$ (the "elementary" symmetric streak), $s = 2p$, and $s = 3p$ are consistent with $v = cs^{-1}$, where $c = (250 \pm 20)$ μm^2/s. These velocities are reduced (but remain constant in time) if a colloidal inclusion detaches together with the streak, as is sometimes observed, and is dragged through the fluid by the end of the streak. They are also reduced when only a part (of thickness s) of the cross section of a thick oily streak retracts; this process occurred frequently especially in thick films.
17. O. D. Lavrentovich, M. Kléman, V. M. Pergamenshchik, *J. Phys. II (Paris)* **4**, 377 (1994).
18. The oily streak network at zero stress maintains its node and link structure. It is, therefore, more analogous to a fixed-network chemical gel than to a physical gel whose network undergoes dynamical rearrangements.
19. A short video of the moving bubble experiment is available at www.physics.upenn.edu/~weitzlab/research/cholesteric.html.
20. Standard theories of elastic networks [L. R. G. Treloar, *The Physics of Rubber Elasticity* (Clarendon, Oxford, 1975)] predict $G_0' \simeq nw/3$, where w is the strain energy of one network element and $n \simeq d_{net}^{-3}$ is their number density. This result is independent of the precise microscopic origin of w. In rubber, this origin is purely entropic, and $w = (3/2)k_BT$. For oily streak defects with line tension $\mathcal{T}$, $w = \mathcal{T}d_{net}$ and $G_0' \simeq \mathcal{T}/d_{net}^2$.
21. The cholesteric pitch was 15 μm in both cases. The materials were rapidly quenched from the isotropic to the cholesteric phase and maintained at 20°C. We

used a double-wall Couette apparatus with gap of 1 mm and measured the frequency dependence of the storage modulus $G'(\omega)$ and loss modulus $G''(\omega)$ in a small-amplitude oscillatory shear experiment.

22. Without preshearing, $G'(\omega)$ and $G''(\omega)$ indicated solid-like behavior similar to that reported for pure smectics (*7*, *8*) but with magnitudes of the moduli three to four orders of magnitude smaller. This result is consistent with the presence of a persistent macroscopically disordered texture of cholesteric layers.
23. Recall that a solid is characterized by $G'(\omega) \rightarrow const \neq 0$ and $G''(\omega) \rightarrow 0$ as $\omega \rightarrow 0$; this implies $G'(\omega) > G''(\omega)$ at sufficiently low frequencies. In a liquid, in contrast, $G'(\omega)/G''(\omega) \rightarrow 0$ as $\omega \rightarrow 0$.
24. In addition to the measurements in the linear viscoelastic regime ($u \leq 0.05$) described above, we measured $G'(\omega,u)$ and $G''(\omega,u)$ at strain amplitudes u up to 0.4 and found $uG'(\omega,u)$ to be practically u-independent for $0.2 \leq u \leq 0.4$ and $\omega \leq 5$ rad/*s*. The low-frequency limit of $uG'(\omega,u)$ in this range of u is the yield stress σ_y, which we measured to be 0.04 dyne. The strain value $u_y \simeq 0.15$ at which $uG'(\omega,u)$ begins to saturate agrees well with $\sigma_y/G'_0 \simeq 0.2$, where $G'_0 = 0.2$ dyne/cm^2 is the elastic shear modulus in the linear regime, thus providing an internal consistency check of our data.
25. We thank T. Martin for participation in the early stages of this project, V. Trappe for help with rheometry, and O. Lavrentovich for useful discussions. This work was supported primarily through NSF grant DMR95-07366, as well as the bourse Lavoisier du Ministère Français des Affaires Etrangères.

11 September 1998; accepted 8 December 1998

Role of Nonexercise Activity Thermogenesis in Resistance to Fat Gain in Humans

James A. Levine, Norman L. Eberhardt, Michael D. Jensen*

Humans show considerable interindividual variation in susceptibility to weight gain in response to overeating. The physiological basis of this variation was investigated by measuring changes in energy storage and expenditure in 16 nonobese volunteers who were fed 1000 kilocalories per day in excess of weight-maintenance requirements for 8 weeks. Two-thirds of the increases in total daily energy expenditure was due to increased nonexercise activity thermogenesis (NEAT), which is associated with fidgeting, maintenance of posture, and other physical activities of daily life. Changes in NEAT accounted for the 10-fold differences in fat storage that occurred and directly predicted resistance to fat gain with overfeeding (correlation coefficient = 0.77, probability < 0.001). These results suggest that as humans overeat, activation of NEAT dissipates excess energy to preserve leanness and that failure to activate NEAT may result in ready fat gain.

Weight gain occurs in healthy adults when energy intake persistently exceeds energy expenditure. Some individuals appear to increase energy expenditure in response to overeating without increasing volitional exercise and thus maintain a stable body weight. This interindividual variation in weight gain with overfeeding (*1*, *2*) suggests that a thermogenic mechanism or mechanisms may be activated to prevent weight gain or obesity.

When humans are overfed, more than 85% of the stored excess energy is deposited as lipid (*3*), primarily triglycerides. Lipid is ideally suited for long-term energy storage in mammals; it is calorie-dense and hydrophobic, so that storage occurs without water accumulation. In the presence of persistent, positive energy balance, enormous quantities of triglyceride can be stored through increases in adipocyte size and number (*4*, *5*). Even lean individuals store enough fat to meet energy requirements for more than 1 month, whereas some obese individuals have fat stores that would exceed energy requirements for a year (*6*, *7*). However, why some people appear to accumulate adipose tissue more efficiently than others is unclear (*8*).

The efficiency of energy storage is calculated by dividing the excess calories stored by the excess calories consumed. Energy storage efficiency can never equal unity because heat transfer is not perfect. An energy efficiency of zero would indicate that all excess energy consumed is dissipated through increased energy expenditure. It has been argued that efficient energy storage is beneficial because it allows longer survival during famine. However, for many Western populations, where food supply is abundant and readily available, efficient energy storage predisposes to obesity, the accumulation of excess body fat. Obesity affects more than one-third of the U.S. population and is a major public health concern because it is associated with diabetes, hypertension, hyperlipidemia, and cardiovascular disease (*9*).

Some humans appear to resist fat gain with overeating, whereas others readily store excess fat. These subjective observations have been confirmed by a small number of clinical studies that document a severalfold interindividual variation in fat accumulation with overfeeding (*1*, *2*, *10*). However, the thermogenic adaptation that allows some individuals to resist weight gain despite overeating has not been identified.

To address this question, we designed a study that allowed us to identify which component or components of energy expenditure showed enough variability to account for the variability in resistance to fat gain during overfeeding. Sixteen nonobese adults (12 males and 4 females, ranging in age from 25 to 36 years) underwent measures of body composition and energy expenditure before and after 8 weeks of supervised overfeeding by 1000 kcal/day. Body composition was measured with dual energy x-ray absorptiometry (DXA) (*11*), and total daily energy expenditure was measured with doubly labeled water (*10*, *12*). The latter procedure required the administration of water containing

Table 1. Energy partitioning in 16 healthy human volunteers who were fed 1000 kcal/day (4.2 MJ) in excess of weight maintenance requirements for 8 weeks. Additional data are available at www.sciencemag.org/feature/data/982662.shl.

Variable (unit)	Mean	Range
Baseline weight (kg)	65.8	53.3–91.7
Overfed weight (kg)	70.5	58.8–93.1
Weight gain (kg)	4.7	1.4–7.2
Fat gain (kcal/day)*	389	58–687
Fat-free mass gain (kcal/day)*	43	15–78
Baseline dietary intake (kcal/day)	2824	2265–3785
Baseline resting energy expenditure (kcal/day)	1693	1470–1990
Overfed resting energy expenditure (kcal/day)	1772	1460–2040
Baseline thermic effect of food (kcal/day)	218	89–414
Overfed thermic effect of food (kcal/day)	354	133–483
Baseline total energy expenditure (kcal/day)	2807	2216–3818
Overfed total energy expenditure (kcal/day)	3361	2508–4601

*Energy contents of tissues were calculated with published constants (*3*).

J. A. Levine and M. D. Jensen, Department of Medicine, Endocrine Research Unit, Mayo Clinic and Mayo Foundation, 200 First Street Southwest, Rochester, MN 55905, USA. N. L. Eberhardt, Departments of Medicine and of Biochemistry and Molecular Biology, Endocrine Research Unit, Mayo Clinic and Mayo Foundation, 200 First Street Southwest, Rochester, MN 55905, USA.

*To whom correspondence should be addressed. E-mail: jensen.michael@mayo.edu